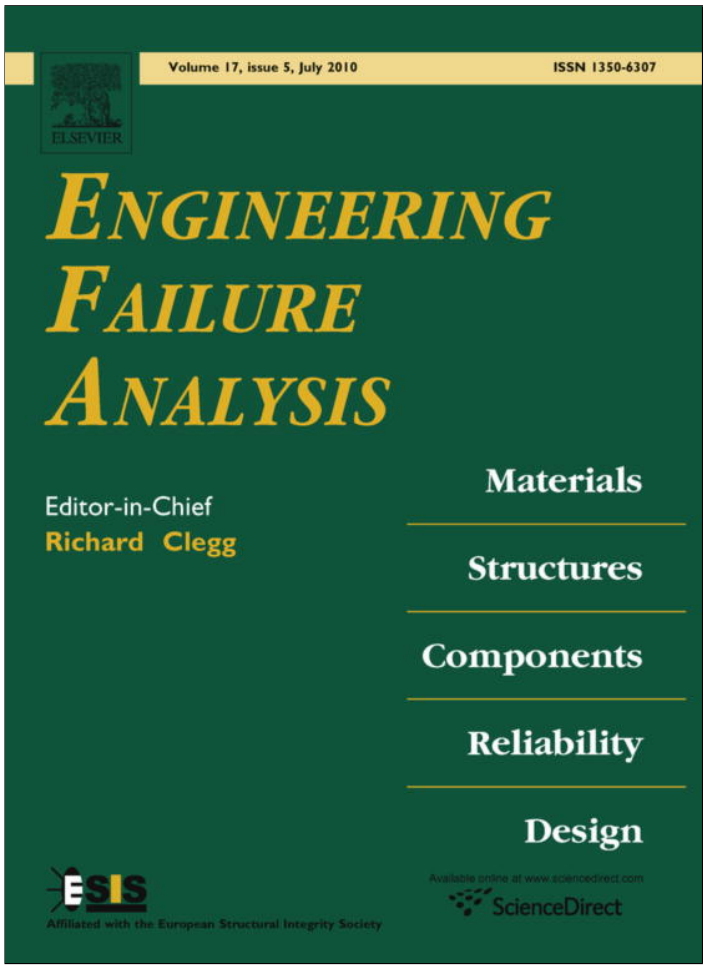

Engineering Failure Analysis 17 (2010) 1038–1050

Contents lists available at ScienceDirect

Engineering Failure Analysis

journal homepage: www.elsevier.com/locate/engfailanal

Analysis of fatigue crack growth and estimation of residual life of the walking beam of an oilfield pumping unit

C. Larrainzar, I. Korin *, J. Perez Ipiña

Grupo Mecánica de Fractura/Laboratorio de Propiedades Mecánicas – Universidad Nacional del Comahue, Buenos Aires St. #1400, Neuquén CP8300, Argentina

ARTICLE INFO

Article history:
Received 18 September 2009
Received in revised form 16 December 2009
Accepted 17 December 2009
Available online 4 January 2010

Keywords:
Residual life
Pump failures
Failure assessment diagram
Fatigue crack growth

ABSTRACT

An analysis of the fatigue crack growth and the corresponding residual life evaluation of the walking beam of an oilfield pumping unit are presented. Lifting lugs had been welded on the upper flange of the walking beam at the moment of assembling the machine. A crack nucleated at one of the weld toes and grew by fatigue up to the critical condition that led up to the instability of the waking beam after 10 years of operation, taking the equipment out of service and producing important economic losses to the operating company.

As the company operates many units working in similar conditions, the estimation of fatigue residual life presents interest in order to define inspection intervals for examinations by non-destructive testing. In this way, any crack growing by fatigue will be detected and repaired, preventing the catastrophic failure of the component.

The stress cycle at the failure zone was calculated and the mechanical properties of the walking beam steel were determined. With this information the final failure conditions were analyzed by using the failure assessment diagram. The fatigue residual life was then estimated by means of a model developed to consider the particular features of the crack path related to the beam geometry. Different operating situations were considered.

Finally, based on the results obtained, an interval of 12 months between consecutive inspections of the examinations by non-destructive testing was proposed.

1. Introduction

A pumping unit is a device conceived to extract oil from the well: an electric motor (or combustion engine) supplies the necessary power to the reciprocating motion of the crank driven mechanism, the movement is transmitted to the walking beam and then to the wireline in order to pump the oil from the depth. Fig. 1 is a schematic representation of the pumping unit with a detail of the failed section. Fig. 2 shows the main dimensions of the pumping unit, according to the manufacturer's technical specifications [1].

Several pumping units were installed at the same reservoir situated in the Patagonian steppe, working for long periods and many times at different operating conditions. Apart from scheduled programmed maintenance stops, the units are also visited, in shorter periods, for visual inspections and verification of their proper operation conditions.

To facilitate the assembly of the machines, and according to information provided by personnel of the company, lifting lugs were welded in the superior flange of the walking beams. These welds were carried out by manual arc welding with no qualified weld procedure nor post-weld heat treatment, Fig. 1. After approximately 10 years operating satisfactorily, the walking beam of one unit broke catastrophically, a short time after a visual inspection had been carried out. A crack

* Corresponding author. Tel./fax: +54 (0)299 4490355.
E-mail addresses: colarrainzar@yahoo.com.ar (C. Larrainzar), ikorin@uncoma.edu.ar (I. Korin), pipina@uncoma.edu.ar (J. Perez Ipiña).

1350-6307/$ - see front matter © 2009 Elsevier Ltd. All rights reserved.
doi:10.1016/j.engfailanal.2009.12.003

Nomenclature

C	constant of the Paris-Erdogan Law
da/dN	fatigue-crack-growth rate
E	Young's modulus
F	wireline load
K	stress intensity factor
K_r	ratio of applied stress intensity factor to material fracture toughness (KI/KIC)
K_I	applied mode I stress intensity factor
K_{IC}	plane-strain fracture toughness
m	exponent of the Paris-Erdogan law
R	stress ratio ($\sigma_{min}/\sigma_{max}$)
L_r	applied stress to plastic collapse stress ratio (σ_{REF}/σ_L)
Y	geometric factor
ΔK	stress intensity factor range
ΔK_{th}	fatigue-crack-growth threshold
$\Delta\sigma$	fatigue stress range
δ	crack tip opening displacement (CTOD)
λ	frequency of the stress cycle
σ_L	plastic collapse stress
σ_m	fatigue mean stress

Abbreviations

BDP	bottom dead point
CTOD	crack tip opening displacement
CMOD	crack mouth opening displacement
FAD	failure assessment diagram
NDT	non-destructive testing
SE(B)	single edge bend specimen
TDP	top dead point

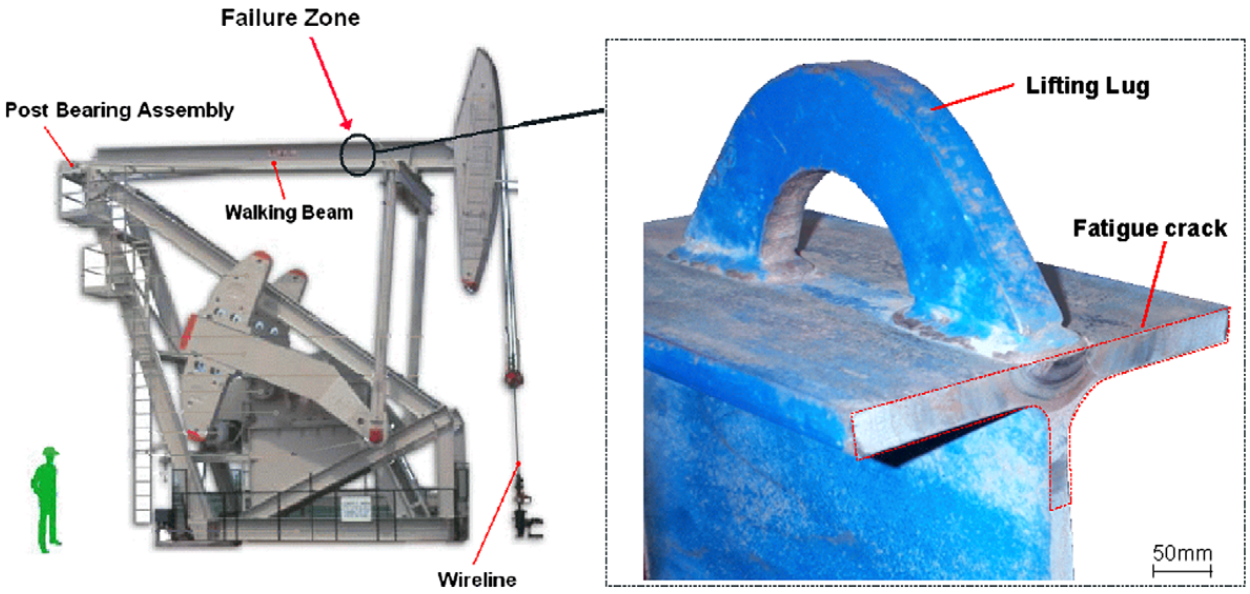

Fig. 1. Oilfield pumping unit scheme and failed section detail.

had initiated at one of the weld toes at the lifting lug (Fig. 1), grew by fatigue until it grew unstably and the walking beam broke in two pieces.

Although the welding procedure has been improved nowadays and the welding of lifting lugs is no longer a problem in new equipment, the company that required this study was concerned with this subject since two failures had already occurred, while several identical pumping units were still operating in similar conditions.

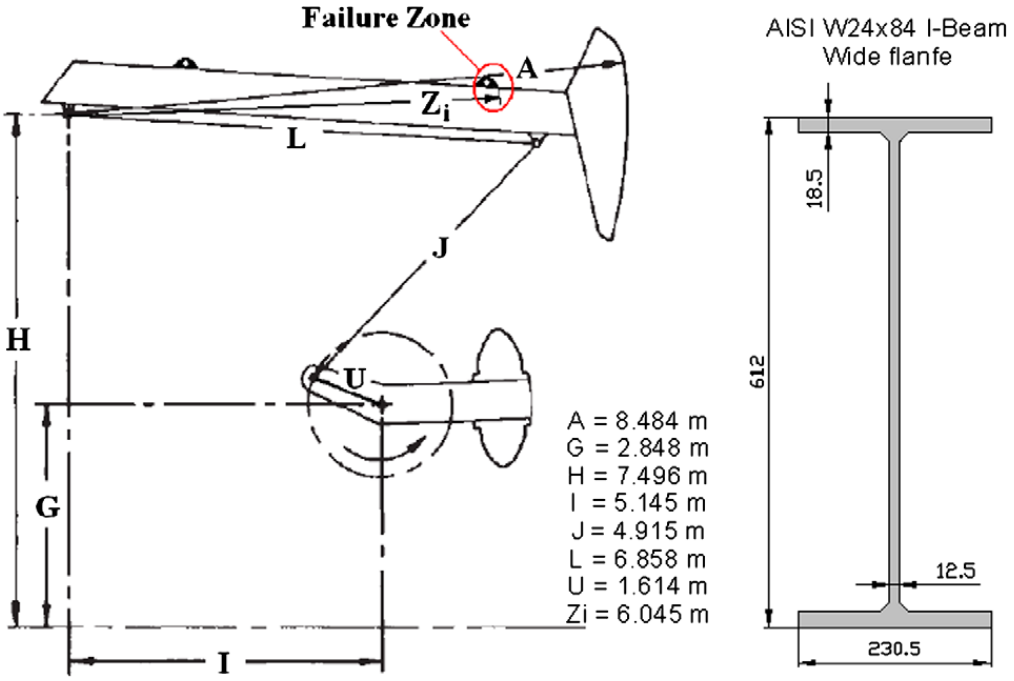

Fig. 2. Dimension data of the pumping unit and walking beam section.

An analysis of fatigue crack growth of the failed walking beam and the study of the residual life of similar pumping units are presented in this work. Several situations were considered and an interval for NDT inspection is proposed.

2. Materials and methods

The failure analysis presented in this work was performed studying several approaches. The load acting in the structure was analyzed in first place. For this purpose all the necessary dimensions and characteristics of the unit were obtained from the technical specifications of the manufacturer or by in situ measurement. Then, the fatigue load on the structure was obtained from a surface card (i.e. the load variation measured in the pumping wireline, see Fig. 1) supplied by the company.

Once obtained the acting loads over the structure, the kinematic chain of the machine was analyzed in order to estimate the loads on the walking beam. Then, the stress cycle in the failure zone was calculated.

The mechanical properties and the type of steel were characterized by means of:

- Chemical composition.
- Tensile tests.
- Fracture toughness tests (CTOD) at different temperatures.

Employing information obtained from these tests, the final failure conditions were analyzed by means of the failure assessment diagram [2].

Then, the fatigue residual life was estimated by means of a model developed to consider the particular features of the crack path related to the beam geometry. This model uses a combination of available stress intensity factor solutions, to provide solutions capable of describing the behavior of the crack in all stages. Besides, the obtained model can be used to predict the crack size 10 years before the failure.

Finally, different operating situations were considered in a variability analysis, and based on these results, an inspection interval for examination by NDT was suggested.

3. Results

3.1. Analysis of the load spectrum

Fig. 3a shows the surface card supplied by the company. Force vs. vertical displacement of the load point at the wireline are indicated in this graphic (see Fig. 1). Fig. 3b shows a more suitable fatigue data representation by using an estimated average speed (i.e. the strokes per minute of the machine) over the past 10 years.

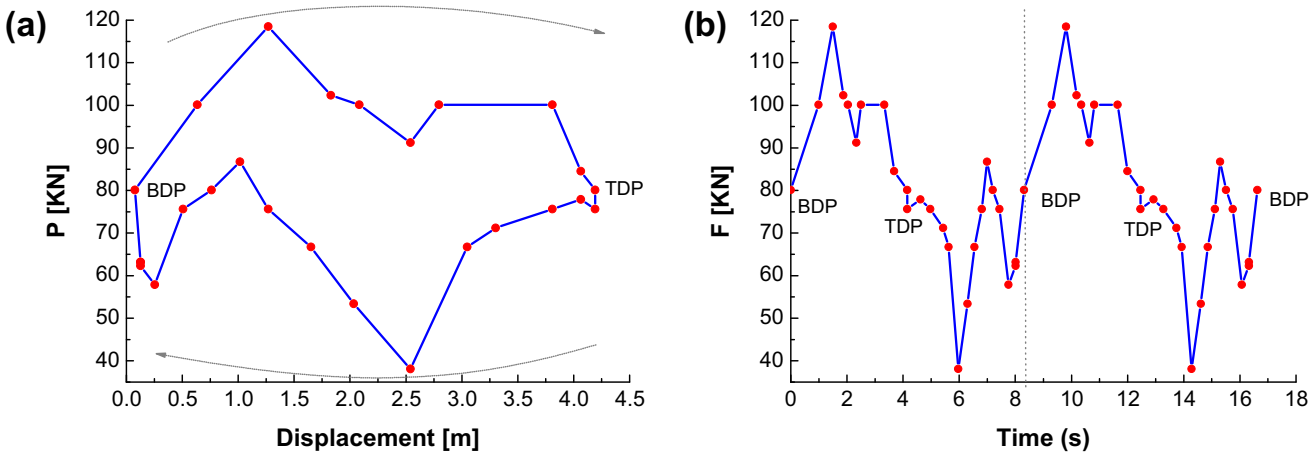

Fig. 3. (a) Surface card of the pumping unit and (b) load spectrum obtained from the surface card.

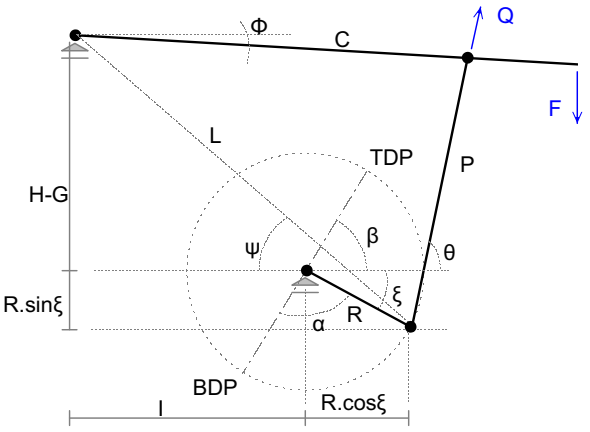

Fig. 4. Scheme of the kinematic chain used for the load analysis.

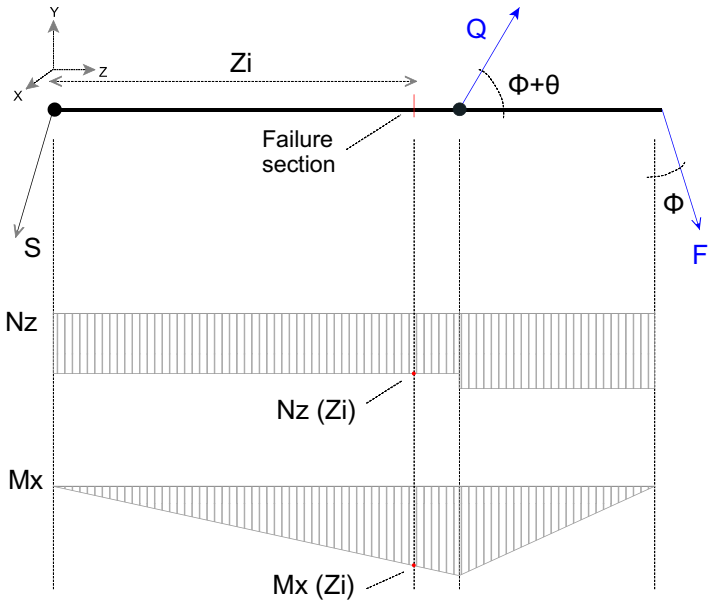

Fig. 5. Load analysis at the walking beam.

3.2. Analysis of the kinematic chain

The kinematic chain of the pumping unit was considered as a four-bar mechanism, as shown in Fig. 4. The angles Φ and θ for the maximum and minimum stresses were calculated as a function of the angle α of the crank because they are necessary to estimate the loads at the walking beam:

$$\theta = 180^{\circ} - \psi - \cos^{-1}\left(\frac{P^2 - L^2 - C^2}{2PL}\right) \tag{1}$$

$$\phi = \sin^{-1}\left[\frac{P\sin\theta - R\sin\xi - (H-G)}{C}\right] \tag{2}$$

where

$$L^2 = [(H-G) + R\sin\xi]^2 + (I + R\cos\xi)^2 \tag{3}$$

$$\psi = tg^{-1}\left[\frac{(H-G) + R\sin\xi}{I + R\cos\xi}\right] \tag{4}$$

and

$$\xi = 180 - \beta - \alpha \tag{5}$$

After the load analysis was solved (see Fig. 5), the stress cycle was estimated at the failed walking beam cross section (see Fig. 2). Fig. 6 shows the stress cycle that corresponds to the load spectrum shown in Fig. 3b. This figure also shows, in dashed lines, the simplified stress cycle used in the fatigue analysis.

3.3. Steel characterization

The walking beam corresponded to an AISI W24x84 wide flange type, and its dimensions were obtained from direct measurement of the component. As there was not available information about the type of steel of the walking beam, a chemical analysis was performed by optical emission spectroscopy. Results are shown in Table 1 and, according to them, the steel corresponds to an ASTM A131/A131 M-04 Grade AH32, or UNS-K 11846 steel [3].

Tension and fracture toughness tests were performed to characterize the mechanical properties of the steel. The specimens were extracted from the web of the beam, close to the failed section. Table 2 shows the tension test results at 25 °C performed according to ASTM E 08-2001 [4].

CTOD tests according to ASTM E 1820-2005 [5] were also performed in order to characterize the fracture toughness at different temperatures. The specimens were the single edge bend type, SE(B), with $W = 24$ mm and thickness-to-height ratio, $B/W = 0.5$, and they were extracted in L–T direction according to ASTM E 1823-2002 [6]. Fig. 7 shows the obtained Load (P) versus the CTOD (δ) records at room and low (−15 °C) temperatures. No brittle fracture occurred at any temperature and then "*maximum load CTOD values*" were obtained as is shown in Table 3, together to their K-equivalent values.

3.4. Analysis of the fatigue crack propagation

As Fig. 9 shows, the crack initiated at the weld toe and grew by fatigue showing classic beach marks. When the crack front attained the web, an unstable crack growth occurred in the web, followed by a crack arrest after about 24 mm of unstable

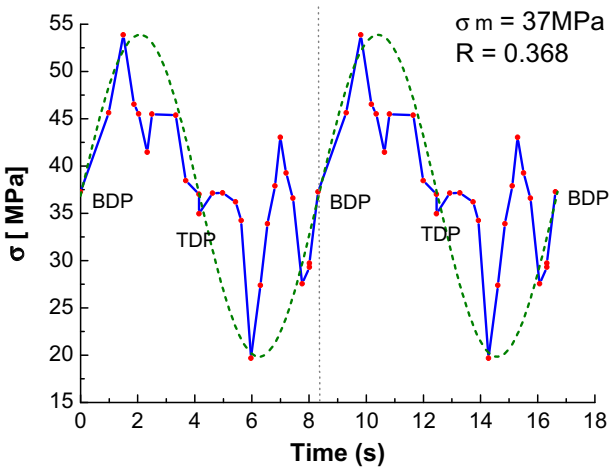

Fig. 6. Actual and simplified stress cycles.

Table 1
Chemical composition of the steel (wt.%).

	C	Si	Mn	Cr	Mo	Ni	Al	Co	Cu	V	W	Pb	Fe
x	0.1	0.278	1.12	0.07	0.02	0.11	0.02	0.02	0.278	0.03	0.05	0.04	97.9
s	0.01	0.01	0.02	0	0	0	0	0	0	0	0.02	0.01	0.05

Table 2
Tension test at 25 °C.

σ_{YS} (MPa)	σ_{UTS} (MPa)	Elongation (%), l_0 = 50 mm
383	490	40
392	488	41

growth, probably as consequence of stress redistribution. Then the crack continued growing by fatigue although with three fronts. This growth continued until the branches corresponding to the flange nearly attained the far ends, and then the branch in the web grew unstably up to the final separation of the walking beam.

In order to carry out the analysis, the crack growth was divided into two stages, as Fig. 9 shows. The first stage ranged from the crack initiation up to the beginning of the first instability. The second stage started at the arrested crack front in the web and the corresponding fronts in the flange, up to the final instability. The terminology used to characterize dimensionally the crack geometry at each stage is shown in Fig. 10.

3.5. First stage of crack growth

In order to estimate the stress intensity factor, the first stage of the crack growth was modelled as a semi-elliptical crack in a finite plate under pure tension [7,8].

Four beach marks were used to obtain the aspect ratio (i.e. a/c) at different points of this stage (Fig. 9).

The stress intensity factor amplitudes, ΔK, were calculated at these marks for the flange direction ($\varphi = 0$, $\varphi = \pi$) and the web direction ($\varphi = \pi/2$). This analysis was performed up to an aspect ratio $a/t = 1$ because it is the limit of the used model. Results are shown in Table 4.

3.6. Second stage of crack growth

After the crack was arrested, it advanced once again by fatigue, now with three fronts, two of them at the flange with opposite directions and the remaining one by the web (see Fig. 9)

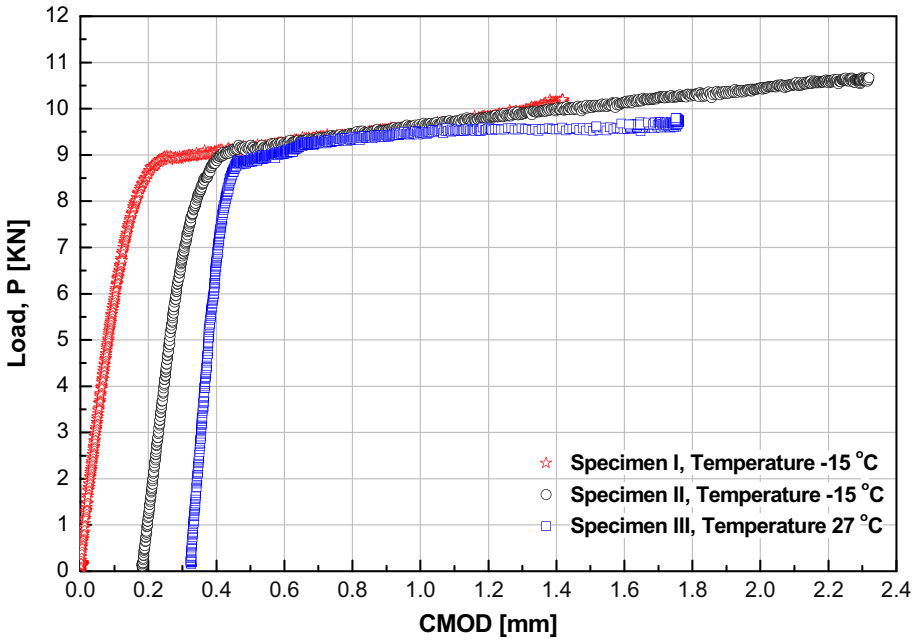

Fig. 7. Load vs. CMOD records for CTOD tests.

Table 3
Results of the fracture toughness tests, CTOD.

Specimen	I	II	III
T (°C)	−15	−15	27
$CTOD_{Pmax}$ (mm)	0.81	0.83	0.71
K_{ICeq} (MPa $m^{1/2}$)	365	367	340

The crack models to estimate the stress intensity factors in this stage were obtained from Ref. [9] and are different for the web and for the flange. A single edge cracked rectangular plate under pure bending g was considered for the web. A center cracked rectangular plate under uniform tension was used for the flange direction up to an aspect ratio $c/w = 0.8$.

The values adopted in this second stage by the stress intensity at the crack fronts were calculated at six points that corresponded to beach marks clearly observed at the fracture surface. The beach marks at both, flange and web, were carefully correlated by visual analysis. Results are shown in Table 5. Using these values the crack growth rates were then estimated.

3.7. Analysis of instability by means of the FAD

The FAD [10] was employed to analyze the final instability. Originally, the FAD considered linear elastic fracture mechanics and plastic collapse as two forms of failure of a cracked component, although nowadays, the newer versions also contemplate the use of elastic–plastic fracture mechanics. Nevertheless, for the present analysis the simplest option adopted by API 579-1/ASME FFS-1 [2] was used.

Two parameters were evaluated for this option, the first one K_r, is given by:

$$K_r = \frac{K_I(a,\sigma)}{K_{IC}} \tag{6}$$

where K_I is the applied stress intensity factor and K_{IC} is the fracture toughness of the material.

The second parameter corresponds to the stress ratio L_r, which is a measure of the proximity to plastic collapse and is given by:

$$L_r = \frac{\sigma_{REF}}{\sigma_L} \tag{7}$$

For this case, and according to the recommendations of API 579-1/ASME FFS-1 [2], σ_L corresponds to the minimum material yield stress σ_{YS}, and σ_{REF} is the applied reference stress load solution for an extended surface crack in a plate under bending, calculated according to Refs. [5,11]. The reference stress σ_{REF} was assessed for the crack sizes shown in Table 5, where the applied stress intensity factors were also estimated. Note that the resisting area of the profile and its moment of inertia decreased as the crack advanced, generating therefore an increment of the reference stress in the remaining ligament.

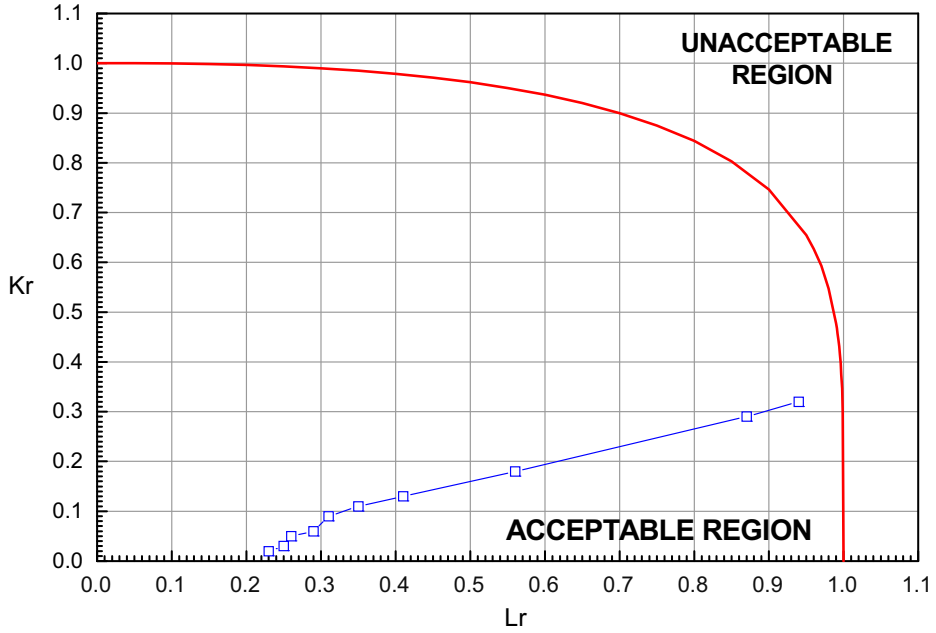

Fig. 8. Crack growth stages definition (up). Instability and details of beach marks (down).

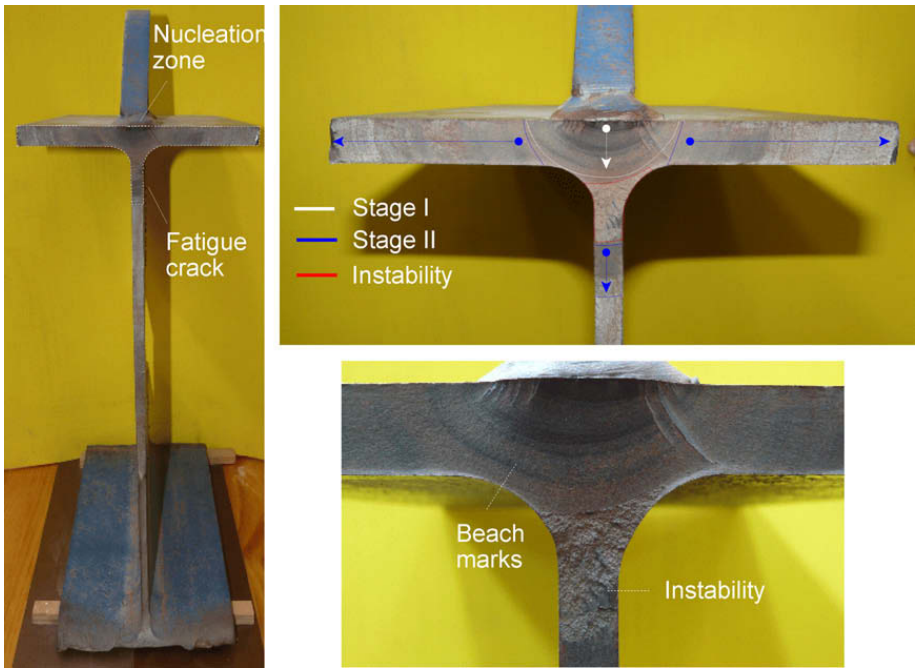

Fig. 9. Crack growth models and nomenclature for both stages.

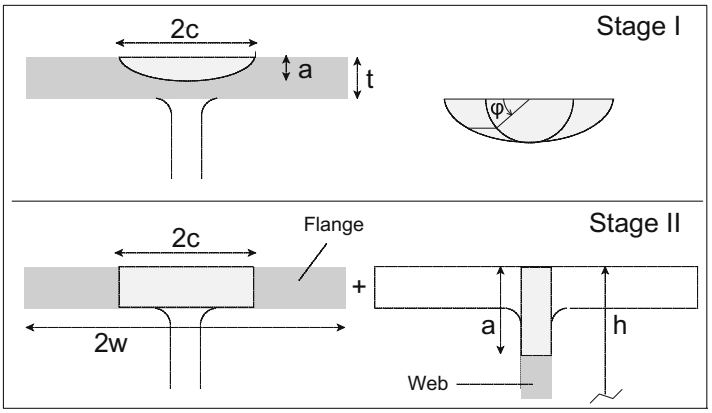

Fig. 10. Failure assessment diagram analysis.

Table 4
Stage I crack growth, embedded semi-elliptical surface crack in a finite plate under tension ($a/t < 1$).

	a (mm)	$2c$ (mm)	t (mm)	a/t	K (MPa m$^{0.5}$), $\varphi = \pi/2$	K (MPa m$^{0.5}$), $\varphi = 0$
Mark 1	4.9	20.6	18.5	0.26	4.78	3.66
Mark 2	11.4	39.9	18.5	0.62	7.64	6.69
Mark 3	18	57.8	18.5	0.97	11.14	10.95
Mark 4[a]	25.6	71.2	18.5	**1.38**	15.39	18.17

[a] Out of range, invalid value.

The FAD defines acceptable and unacceptable regions of a component, separated by a line given by the following equation:

$$K_r = \left(1 - L_r^{2.5}\right)^{0.20} \tag{8}$$

The material fracture toughness required to the FAD was estimated from the CTOD tests, by mean of:

$$K_{IC} = \sqrt{mE\sigma_{YS}\delta_m} \tag{9}$$

Table 5
Stage II crack growth, center cracked rectangular plate under uniform tension, $c/w < 0.8$ (flange); single edge cracked pure bending specimen, $a/h < 0.6$ (web).

Flange					Web			
Mark	$2c$ (mm)	$2w$ (mm)	c/w	K (MPa m$^{0.5}$)	a (mm)	h (mm)	a/h	K (MPa m$^{0.5}$)
Mark 5	71.2	230.5	0.28	20.23	49.6	612	0.08	19.83
Estimated	95.4	230.5	0.41	27.14	57.05	612	0.09	23.15
Mark 6	126	230.5	0.55	40.16	64.5	612	0.11	28.44
Estimated	176	230.5	0.76	89.8	67.75	612	0.11	40.74
Mark 7[a]	226	230.5	**0.98**	263.92	71	612	0.12	65.61

[a] Out of range, invalid value.

where δ_m corresponds to the CTOD values indicated in Table 3, E is the material Young modulus (210 GPa), σ_{YS} is the yield stress and m is a constant that can take values between 1 and 3 [2,10]. The estimated values of K_{IC}, for $m = 2$, are shown in Table 3.

Because it was the minimum, the estimated K_{IC} value at 27 °C was used to calculate the K_r values.

Fig. 8 shows Eq. (8) and the points corresponding to the values of K_r and L_r on the web, for the different crack sizes shown in Table 5. The performed FAD analysis showed that the walking beam failure was probably due to plastic collapse rather than brittle fracture.

3.8. Estimation of the fatigue residual life

In order to perform the analysis of residual life, several assumptions were adopted: Linear Elastic Fracture Mechanics validity, and sinusoidal stress cycle with increasing amplitude as the crack grows. The fatigue crack propagation rates were calculated without considering the existence of stress concentrations and residual stress fields in the welded zone. Threshold effects, overloads or stops, or different-to-sub-critical fatigue crack growth mechanisms were not considered either.

In this way, a model based in the Paris-Erdogan assumptions was used:

$$\frac{da}{dN} = C\Delta K^m = 6.89 \times 10^{-9}\Delta K^3 \tag{10}$$

The constants C and m employed in Eq. (10) were extracted from Refs. [12,13], and correspond to ferritic-perlitic steels at room temperature in air or another non-aggressive environments.

Fig. 11a shows the crack size evolution through the web and the flange for both stages for a period of 120 months up to the fracture. The actual sizes obtained from the beach marks are also indicated in the figure. In order to compare easily different situations, the results were plotted in a relative time scale, "*t - tfailure*", where the moment of collapse corresponds to a null value. The figure includes reference lines representing crack sizes of interest at the flange ($\varphi = 0$) i.e. the NDT detectable size and the crack sizes that correspond to the fatigue thresholds of 2 MPa m$^{0.5}$ and 5 MPa m$^{0.5}$. Fig. 11b shows in detail the last 10 month before collapse. At the web, the first instability took place over the end of the stage I and the collapse occurred for a final crack size of 71 mm. Instead, at the flange, the collapse occurred for a crack size of 226 mm (nearly cross over section).

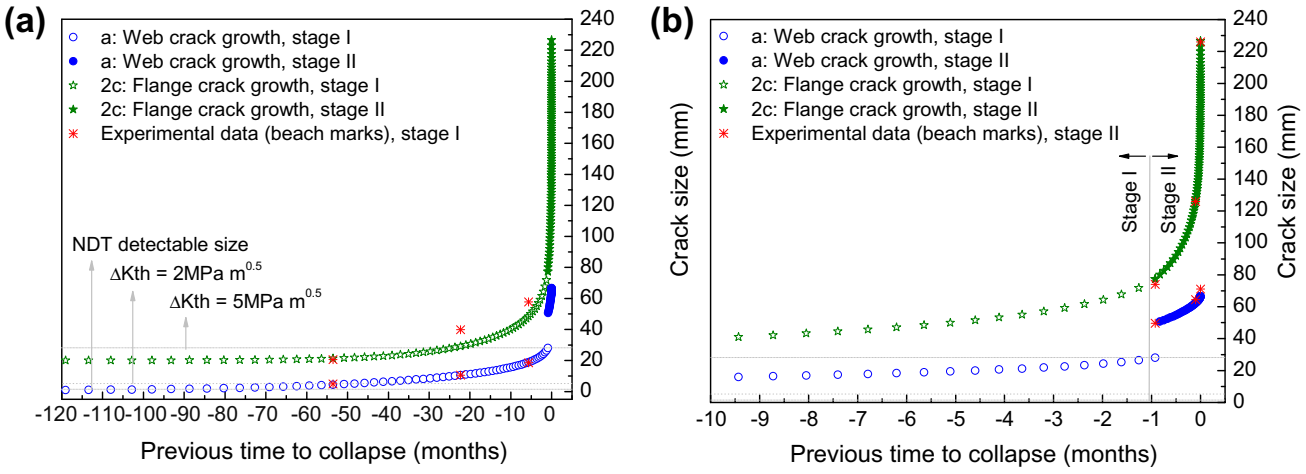

Fig. 11. Crack growth model and reference beach marks.

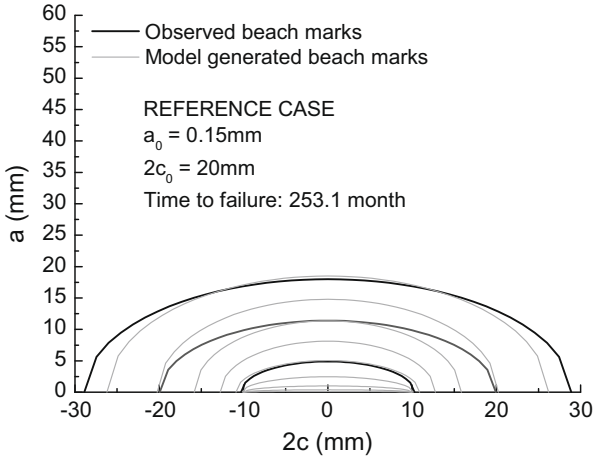

Fig. 12. Comparison of crack size estimation by the model and beach marks at the fracture surface.

The probable crack size 120 months before the failure was estimated by the model and the aspect ratio was verified comparing the predicted crack with the closest beach mark at the fracture surface. The crack size capable to fulfil the best fit between the actual and the generated beach marks was obtained by using an iterative process. Results are shown in Fig. 12.

3.9. Variability analysis

The above analyzed situation corresponds approximately to the operating conditions of the broken equipment at the failure time. As this kind of pumps can experience other conditions during operation, a variability analysis was performed: in load and frequency, from the minimum to the maximum recommended by the manufacturer. Other parameters that influence the fatigue residual life are the constants of the Paris-Erdorgan law, being the used values considered as conservative. Then, a value 10% lower for m and a larger value of C (16.5) were also analyzed. Table 6 displays the values considered and Figs. 13 and 14 show the estimated crack sizes as function of the previous time to the collapse for the different cases. The base case and the most unfavorable case (case 7) are shown in full line and full-circle points, respectively.

Table 6
Considered cases in the variability analysis.

Cases	$\Delta\sigma$ (MPa)	$C \times 10^{-09}$	m	λ (Hz)
Base case	37	6.89	3	0.12
Case 1	44.2	6.89	3	0.12
Case 2	25.9	6.89	3	0.12
Case 3	37	16.5	3	0.12
Case 4	37	6.89	2.7	0.12
Case 5	37	6.89	3	0.07
Case 6	37	6.89	3	0.17
Case 7	44.2	16.5	3	0.17

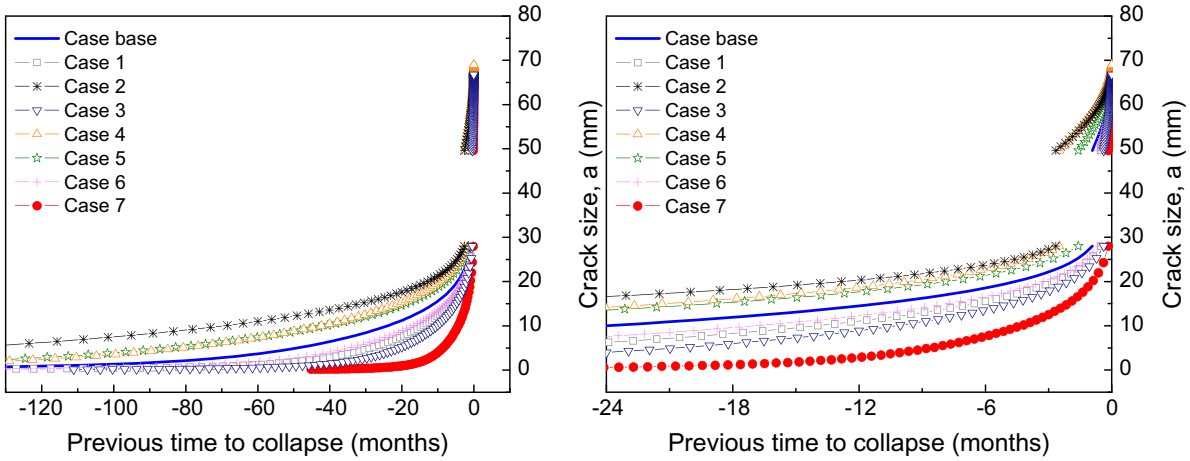

Fig. 13. Variability analysis: crack depth a at the web vs. previous time to collapse.

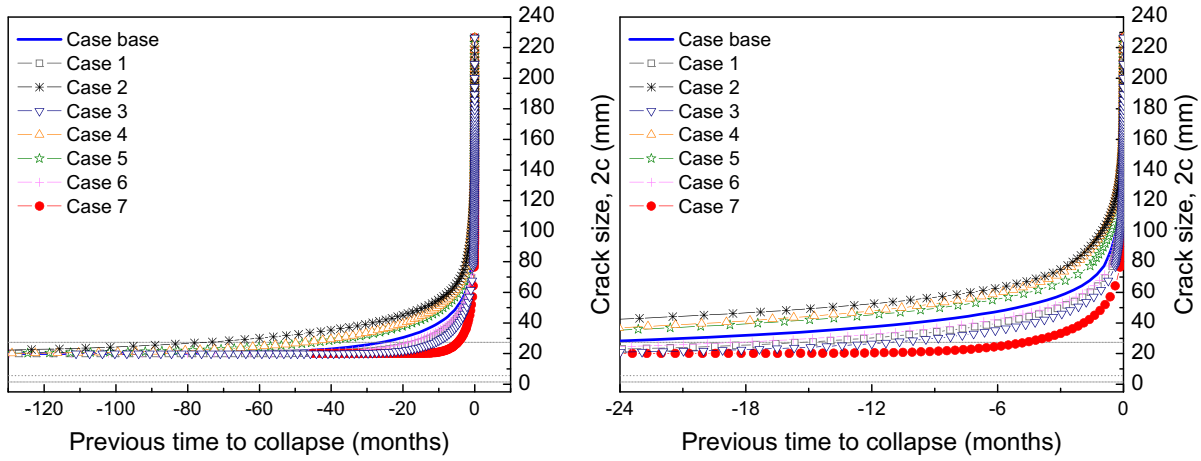

Fig. 14. Variability analysis: crack $2c$ at the flange vs. previous time to collapse.

4. Discussion

Welding lifting lugs to the walking beam without a qualified procedure was the ordinary assembly procedure used by the company 10 years ago and there are still many units welded in this way. However, a qualified procedure is used nowadays in new equipments and also when old units with detected cracks are repaired. However, damage generated during the last 10 years of operation could have created still no detected cracks in more units, and then a study about the remaining life is completely justified because NDT inspections must be carried out in periods lower than that a crack grows from the NDT threshold size up to the critical one.

As was already described, the weld bead gave place to the crack nucleation. The crack grew by fatigue up to the critical condition and the structural instability of the walking beam took place, leaving out of service the machine. The probable factors that took part in the nucleation were: stress concentration in the welded joint, presence of initial small defects in the filler metal, modification of the microstructure and residual stress fields.

CTOD tests were carried out at different temperatures (−15 °C and 27 °C) to characterize the steel fracture toughness because, according to the information received from the company, the failures occurred in winter, with minimum temperatures that can attain −15 °C. The possibility of a brittle failure because the steel was working in the ductile-to-brittle region was discarded after testing because the CTOD results showed that the steel was working in the upper shelf region at all working temperatures.

From the analysis performed on the FAD, a condition very close to the failure line near the plastic collapse axis was predicted, so it can be concluded that the final failure took place by plastic collapse instead of brittle fracture. This result was in accordance with both the observed fracture and the fracture toughness tests results. Although the rupture point should fall outside the acceptable region, this deviation could be attributable to the model used to calculate the reference stress, which does not represent exactly the component geometry.

Referred to the fatigue analysis of the base case, the model predicted a crack size of $2c_0 = 20$ mm. 120 months before collapse. In most of stage I, the crack growth rate (predicted and shown by the beach marks) was larger towards the web direction (a) than in the flange ones ($2c$). Moreover, for the smaller crack sizes, the crack growth rate in the a direction was a lot larger than for the $2c$ directions, with an important change in the crack aspect ratio. At the end of the stage I the tendency changed and the crack growth rate was larger in the flange direction. The used model proved to be accurate enough as it predicted crack aspect ratios in accordance with the observed beach marks. For the last part of stage I, the accuracy diminished for the crack growth rate prediction (da/dN) when the crack was near the opposite border, then the values used in the analysis were those corresponding to the growth in the flange direction.

The analyzed second stage showed that the fronts that advanced for the flange had a larger crack growth rate than the front advancing through the web. This is in accordance with the beach marks and the values of ΔK in Table 5, where the crack growth rate was always larger at the flange than at the web. On the other hand, when the crack was attaining the far borders of the flange, the values of ΔK_{max} seem to be large enough to be out of small scale yielding conditions and then the Paris-Erdorgan law might be out of limits and then inapplicable.

This predicted crack size 120 months before failure resulted much larger than the NDT threshold size ($2c = 1.5$ mm) that the company estimated could be detected. Although it is not easy to explain this inconsistency, it could be related to two causes: the complicated location where the NDT must be performed (see Fig. 1), and the possibility that the defect of $2c_0 = 20$ mm was consolidated from various smaller initial cracks along the weld joint. The last hypothesis is supported by the presence of ratchet marks on the fracture surface (see Fig. 9).

As it was described before, a variability analysis was carried out. The variations in the parameters shown in Table 6 imply that the crack sizes corresponding to 120 months before the collapse are different for every case, i.e. the more severe condition, the smaller crack size (see Figs. 13 and 14). In order to evaluate the effect of each case over the residual life, another

analysis can be performed: considering the same initial crack size for all the cases, and the same final crack size (i.e. the failure crack size), the variations of residual life between the different situations can be evaluated. In this way it was found that: when the fatigue maximum stress was increased in 20%, the fatigue residual life decreased notably, around 40%. When the operating regime of the unit was increased from 0.12 Hz to 0.17 Hz, the fatigue residual life decreased approximately 30%. For a change in the value of the constant C in the Paris-Erdorgan law the residual life decreased around 58%. A decrement of 10% in the value of the coefficient m implied a lower crack propagation rate for the same ΔK and this implied an increment of 25% in the residual life. Finally, the combination of the most unfavorable variables (case 7) implied that the fatigue residual life decreased 80% referred to the base case. Although this last case corresponds to the most demanding combination for the fatigue residual life, it is not very probable.

As expected, stage I occupied far more cycles than stage II, moreover, in most analyzed situations stage II lasted less than three month, which can be considered a too short period for field NDT in this kind of equipment and then the crack must be detected when it still is in stage I.

The analyzes already discussed were performed considering no threshold for the crack growth rate. Considering the threshold recommended by Ref. [2] for this situation, $\Delta K_{th} = 2$ MPa $m^{1/2}$, the corresponding crack sizes are of the order of those that were present at the beginning of Stage I. The crack sizes corresponding to this situation are very small compared to those used in the analysis of the NDT inspection periods, and then were not considered as important for the purpose of this work.

4.1. Proposal of NDT inspection periods

In order to operate the equipment in a reliable way, the most important output for the company, was to establish periods between inspection that assure that any crack that is growing by fatigue will be detected before it reaches its critical size. Then, the most unfavorable condition, case 7, was selected to estimate the time between inspections.

Accepting half of the fatigue life as the intervals between NDT inspections, they could be carried out every 18 months. Nevertheless, in order to cover other situations that require shorter inspection periods, a 1 year period between inspections is proposed. In this way there is not possibility, between two consecutive inspections, that a non-detected crack can grow up to the critical size and produce the collapse of the structure. The inspections should be carried out with a NDT method capable to detect 20 mm or smaller surface crack sizes and in particular they must be especially careful at the lifting lug weld joints.

5. Conclusions

- The lifting lug weld joint was the origin of the initiation and propagation of the crack.
- The final failure was by plastic collapse once the crack crossed the flange of the walking beam nearly completely, as shown by the FAD analysis.
- The predicted crack size 120 months before the failure resulted, for all the cases studied, much larger than the NDT threshold ($2c = 1.5$ mm) the company estimated could be detected.
- A period of inspection of 12 months was recommended for NDT evaluations that ensure a level of crack detection of 20 mm or smaller.
- This period between inspections is recommended for walking beams of pumping units with similar characteristics and operating under conditions contemplated in this work.

Acknowledgements

To ANPCyT (National Agency of Scientific and Technological Promotion) and CONICET (National Council for Scientific and Technological Research) for their financial support. To Mr. Héctor Pérez of Petrolera Entre Lomas S.A. for his collaboration and Mr. Eduardo Benotti of LPM/GMF for his permanent collaboration.

References

[1] Lufkin Oilfield Products Group. General catalog; 2004.
[2] API 579-1/ASME FFS-1. Fitness-for-service, Part 9 and Annex F. 2nd ed.: American Petroleum Institute; 2007.
[3] Properties and Selection: irons, steels, and high performance alloys. ASM handbook, 10 ed., vol. 1. ASM International; 1990.
[4] ASTM E8. Standard test method for tension testing of metallic materials. Annual Book of ASTM Standards; 2001.
[5] ASTM E 1820. Standard test method for measurement of fracture toughness. Annual Book of ASTM Standards; 2005.
[6] ASTM E 1823. Standard terminology relating to fatigue and fracture testing. Annual Book of ASTM Standards; 2002.
[7] Newman JC, Raju IS. Stress-intensity factors equations for cracks in three dimensional finite bodies. In: Lewis JC, Sines G, editors. Fracture mechanics: fourteenth symposium. Theory and analysis ASTM STP 791, vol. I. American Society for Testing Materials; 1983. p. I-238–65.
[8] Lin XB, Smith RA. Finite element modelling of fatigue crack growth of surface cracked plates. Part III: stress intensity factor and fatigue crack growth life. Eng Fract Mech 1999;63:541–56.
[9] Murakami Y. Stress intensity factors handbook, vols. 1 and 2. Oxford: Pergamon Press; 1987.

[10] Perez Ipiña J. Mecánica de Fractura. Buenos Aires: Alsina; 2004.
[11] Lei Y, Budden P. Limit load solution for plates with embedded cracks under combined tension and bending. Press Vess Pip 2004;81:589–97.
[12] Barson JM, Rolfe ST. Fracture and fatigue in structures: applications of fracture mechanics. 3rd ed. West Conshohocken (PA): ASTM; 1999.
[13] Anderson TL. Fracture mechanics, fundamentals and applications. 2nd ed. Boca Raton (Florida, NW): CRC Press; 1995.